Electronic Properties of Sulfur Covered Ru(0001) Surfaces

Michele Pisarra,[†] Cristina Díaz,[†,‡,¶] Ramón Bernardo-Gavito,[§,‖,⊥] Juan Jesús Navarro,[‖] Andrés Black,[§,‖] Fabian Calleja,[‖] Daniel Granados,[‖] Rodolfo Miranda,[‡,§,‖] Amadeo L. Vázquez de Parga,[‡,§,‖] and Fernando Martín[*,†,‡,‖]

†*Departamento de Química, Módulo 13, Universidad Autónoma de Madrid, 28049 Madrid, Spain*

‡*Condensed Matter Physics Center (IFIMAC), Universidad Autónoma de Madrid, 28049 Madrid, Spain*

¶*Institute for Advanced Research in Chemical Sciences (IAdChem), Universidad Autónoma de Madrid, Cantoblanco 28049, Madrid, Spain*

§*Departamento de Física de la Materia Condensada, Módulo 3, Universidad Autónoma de Madrid, 28049 Madrid, Spain*

‖*Instituto Madrileño de Estudios Avanzados en Nanociencia (IMDEA-Nanociencia), Cantoblanco 28049 Madrid, Spain*

⊥*Current address: Physics Department, Lancaster University, LA1 4YB, UK*

E-mail: fernando.martin@uam.es

Phone: +34 914974019

Abstract

The structural properties of sulfur superstructures adsorbed on Ru(0001) have been widely studied in the past. However, much less effort has been devoted to determine their electronic properties. To understand the connection between structural and electronic properties, we have carried out density functional theory periodic boundary calculations mimicking the four long range ordered sulfur superstructures identified experimentally by means of scanning tunneling microscopy (STM) techniques. Our simulations allow us to characterize the nature of the sulfur-Ru bond, the charge transfer between the Ru substrate and the sulfur adlayers, the interface states, as well as a parabolic state recently identified in STM experiments. A simple analysis, based on a one-dimensional model, reveals that this parabolic state is related to a potential well state, formed in the surface when the concentration of sulfur atoms is large enough to generate a new minimum in the surface potential.

1 Introduction

The very rich phase diagram found in the superstructures of Sulfur adsorbed on Ruthenium(0001) has attracted much attention during the 90's. At that time, both experimental studies and theoretical studies[1–7] focused on the development of structural models aimed at explaining the different long range ordered phases of the system, which is characterized by both ordered and disordered sulfur superstructures. Such a versatile interface has recently received renewed interest, mostly because sulfur, similarly to other electronegative non-metals such as oxygen,[8] can be successfully intercalated in the Graphene Ru(0001) interface.[9] In fact the Graphene-S-Ru system, with a controlled amount of intercalated S atoms, may lead to a tunable doping of a quasi freestanding graphene layer, as already observed, for example, in the intercalation of Silicon oxide.[10] Furthermore, the intercalation of S in the Graphene-Ru system opens the possibility of having an ordered intercalated structure, which breaks the hexagonal symmetry of the system.

Despite the detailed knowledge of the structural properties acquired for S-Ru systems, significantly less effort has been devoted to the determination of its electronic properties. Density functional theory (DFT) has been applied to characterize the density of states (DOS) of some of the two-dimensional long range ordered structures formed by sulfur on transition metal surfaces.[11,12] Very recently, a scanning tunneling spectroscopy (STS) study carried out on different S-Ru interfaces has revealed a rich scenario.[13] This work has focused on the empty part of the electronic spectrum, reporting spectral features assigned either to interface states or to potential well states, which exhibit a peculiar dependence on the sulfur coverage. However, to the best of our knowledge, there is no work analyzing the filled part of the band structure for the S-Ru interfaces.

Our aim in this work is investigating the connection between structural and electronic properties by studying the electronic bands of the S-Ru interface. On the one hand, we report the complete band structure for the long range ordered S-Ru interfaces, revealed by Scanning Tunneling Microscopy (STM) measurements. We focus our attention on the hybridization of the sulfur atomic orbitals with the Ru derived bands, which, as already found for weakly bound overlayers on transition metals,[14] could take place in specific parts of the Brillouin Zone (BZ). For the S-Ru interfaces we find that a band mixing takes place over the entire BZ and suggests that a covalent S-Ru interaction is the binding mechanism of the S atoms over the surface. Such a strong interaction is also at the basis of an important and coverage dependent charge transfer from the Ruthenium surface to the S adlayer. This fact implies that, depending on the density of S atoms, the system could exhibit different chemical behaviors when interacting with other molecules or adlayers. We also analyze the puzzling behavior of the potential well state, which is not present for low coverage[13] and exhibits a counterintuitive coverage dependent energy blue shift. In this work we show that this unusual behavior can also be explained by means of a simple one dimensional model.

Potential well states, actually image potential states, have been already reported for 2D materials, like monolayer and few-layers graphene.[15–17] Similar potential well states (also

called super-atom states) have been reported for lower dimensionality systems like 1D carbon nanotubes[18] and fullerene molecules.[19] Even though they cannot participate in the formation of bonds, potential well states are particularly interesting, since they can combine with one another when monolayers are assembled to form layered solids, as in the case of the interlayer state of graphite,[20] or more complex heterostructures. More importantly, they play a significant role in determining the empty spectrum of those systems, which is usually probed by two-photon spectroscopy[15] or STS measurements,[17,21] or other out-of-equilibrium processes that directly involve the empty states of the system.[22,23]

The paper is organized as follows. In the next section we explain the details of our DFT calculations and the experimental set up used for the STM measurements.

In the Results section, we focus on the long range ordered S-Ru interfaces. First of all, we review the structural properties of the S-Ru interfaces (section 3.1), showing the STM topography and presenting the result of the DFT geometry optimizations. Then we study the S-Ru interaction mechanism based on the study of the charge transfer from the ruthenium surface to the S atoms (section 3.2). We complete our analysis, in section 3.3, by studying the electronic properties of each system. In particular we present the band structures of the S-Ru interfaces focusing on the interface states and we compare them with the band structures of S monolayers, obtained by peeling the S atoms off the Ru surface, which allows us to identify similarities and differences between the isolated S monolayers and their Ru-adsorbed versions. In the Discussion section, we analyze in detail the parabolic state found in the S-Ru calculations and present a simplified one-dimensional model to account for its main features. Finally in section 5 we summarize the conclusions.

2 Methods

2.1 DFT calculations

Our DFT calculations rely on the Projector Augmented Wave (PAW) method,[24] as implemented in the plane wave based code VASP,[25] using the PBE[26] exchange-correlation functional, and a plane waves cut off of 400 eV. The S-Ru interface is modeled by a 5-layer Ru (0001) slab with S atoms adsorbed on one side. Four different adsorption geometries have been analyzed, with a surface coverage ranging from $\eta = 0.25$ to $\eta = 0.5$ (see section 3.1). The slab is then periodically repeated in the direction perpendicular to the surface (as it is customary in plane wave based codes) with a lattice constant $L_z = 70$Å, which results in a vacuum distance of ~ 60Å. These choices ensure a negligible interaction between the system replicas and a reasonably good description of the surface/interface states. We checked the reliability of the results performing control calculations, for the system with the smallest in plane unit cell, increasing the numner of Ru layer up to 11 and also using symmetric slabs.

The adsorption sites for each surface coverage were obtained by a full relaxation of the coordinates of the S atoms. During the relaxation process the atoms of the two-topmost Ru layers were also allowed to move. The effect of weak dispersion forces was taken into account using the Tkatchenko-Scheffler method.[27] BZ integrations for the geometry optimization have been carried out using Γ-centered Monkhorst-Pack (MP) grids,[28] characterized by a $\Delta k \lesssim 0.1$Å^{-1}. The relaxed slabs were then used as starting geometries for electronic structure and density of states calculations using MP meshes of $\Delta k \sim 0.03$Å^{-1}. Similar parameters have also been used to carry out calculations for the bare Ru slabs and the S monolayers.

2.2 STM measurements

Experiments have been carried out in a ultra-high vacuum (UHV) chamber, which base pressure is 5×10^{-11} mbar. Our experimental setup is equipped with a low-temperature STM, as well as facilities for tip and sample preparation and analysis. The W tips have been

prepared by Ar^+ sputtering (2.5 keV) in UHV for 45 minutes and resistive heating at high temperature.[29] The Ru(0001) single crystal have been cleaned and flattened by a series of annealing (1400 K) and Ar^+ sputtering (1.4 keV) cycles. The adsorption of the sulfur atoms have been achieved by exposing the crystal sample (kept at 500 K) to a partial pressure of H_2S. The different structures discussed throughout this work have been obtained by varying the exposure time from 45 to 180 seconds, and the pressure from 2×10^{-9} to 2×10^{-7} mbar.[30] All the STM measurements have been carried out at room temperature.

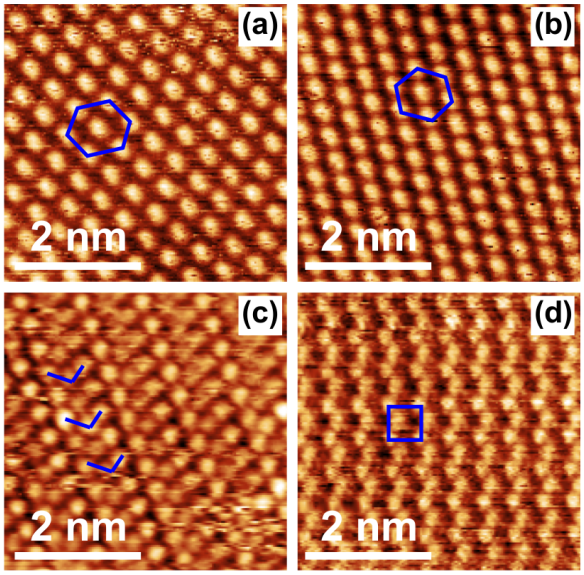

Figure 1: Experimental results. STM topography of long range ordered S atom arrangements (bright spots) obtained exposing a clean Ru(0001) surface to H_2S; the resulting surface coverage is $\eta = 0.25$ (a), $\eta = 0.33$ (b), $\eta = 0.43$ (c), $\eta = 0.50$ (d); the blue lines are a guide to the eye to help out comparison with Fig.2. All images were measured at room temperature, bias voltage 1 V and tunneling current 30 nA.

3 Results

3.1 Structural properties

In past studies of S adsorption on Ru(0001)[31] several atomic arrangements in the sub-monolayer regime were reported, each one characterized by a surface coverage ranging from $\eta = 0.25$ to $\eta = 0.58$. After $\eta = 0.58$, further exposition to H_2S results in the formation

of two-layer structures. In Fig.1, we show topographic images of four long-range ordered structures of S atoms (bright spots) on the Ru surface, found after exposition of the clean Ru surface to increasing dose of H_2S. The surface reconstruction obtained with the smallest dose of H_2S is shown in Fig.1(a) and exhibits hexagonal symmetry. Its unit cell vectors are parallel to the Ru(0001) surface vectors with double length, hence we have a $p(2 \times 2)$ reconstruction and $\eta = 0.25$. Increasing the H_2S dose, we find another hexagonal phase (Fig.1(b)); this time the unit cell vectors exhibit a 30 degree rotation with respect to the Ru surface vectors, i.e. they form the $p(\sqrt{3} \times \sqrt{3})R30$ surface reconstruction. Increasing the S coverage further, several disordered phases appear in which $p(\sqrt{3} \times \sqrt{3})R30$ islands are separated by lines of higher sulfur density called domain walls. The typical size of the islands, (hence the typical distance between the domain walls) decreases as the sulfur coverage increases up to the crytical $\eta = 0.43$ value in which the minimum domain walls distance is realized and a new long range ordered phase appears (Fig.1(c)). This particular surface reconstruction, in which sulfur forms long stripes of "v" arranged atoms, is called Domain Walls close packed (DWcp). Finally, increasing the exposition further, we find a rectangular arrangements of S atoms on the surface (Fig.1(d)); this surface reconstruction is characterized by a unit cell that contains eight Ru atoms and it is called $c(2 \times 4)$ (see also Fig.2).

Guided by the STM results, we have performed DFT calculations for the four long range ordered structures observed in the experiments; the final atom arrangements with the unit cells and Brillouin Zones are given in Fig.2 Our results show that in the two hexagonal phases the S atoms are adsorbed in *hcp* sites of the Ru(0001) surface. For the $p(2 \times 2)$ geometry (Fig.2a), the unit cell consists of one S atom and four Ru atoms per layer, whereas for the $p(\sqrt{3} \times \sqrt{3})R30$ one, we have one S atom and three Ru atoms per layer (Fig.2b), resulting in $\eta = 0.33$. For the DWcp geometry, the most stable configuration of atoms is obtained with a minimum unit cell formed by seven Ru atoms per layer and three S atoms (Fig.2c), two adsorbed in *hcp* sites and one adsorbed on a *fcc* site; this results in a surface reconstruction

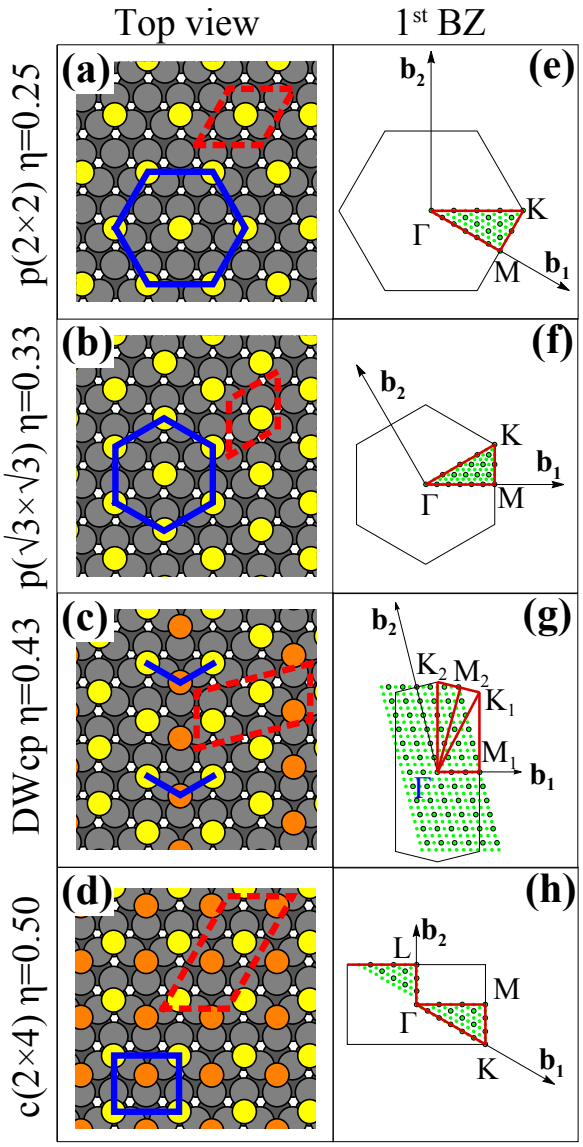

Figure 2: Geometry information: (a-d) Hard-ball model (top view) of the investigated adsorption geometries. Only the two topmost layers of Ru atoms are visible and are shown as gray and black spheres, respectively; yellow circles represent S atoms adsorbed on *hcp* sites whereas orange circles represent S atoms on *fcc* sites. The red dashed line marks a possible choice for the 2D minimal unit cell, whereas the blue line is a guide to the eye to ease the comparison with STM measurements of Fig.1. (e-h) reciprocal space information: 1^{st} BZ, reciprocal lattice vectors, and the high symmetry points used in the DFT calculations; the black or green points mark the k-point meshes used for the BZ integration in, respectively, the geometry optimizations or the self-consistent calculations; the red lines mark the BZ path used in the band plot of Fig.4 and Fig.5.

of $\eta = 0.43$. Finally the rectangular reconstruction is characterized by a unit cell made of eight Ru atoms per layer and four S atoms ($\eta = 0.50$), the latter are adsorbed in equal number on *hcp* and *fcc* sites (Fig.2d).

Table 1: Additional geometry information: d_{S-Surf} is the average distance of the S layer from the topmost Ru layer; d_{A-B} indicates the interatomic distance between atoms A and B; In the 5^{th} column the maximum displacement of the Ru atoms from their nominal position is shown. In the last row, the corresponding values for the RuS_2 system are given for comparison.

Geometry	η	d_{S-Surf}	Min(d_{S-Ru})	Min(d_{S-S})	Max Ru displ.
$p(2 \times 2)$	0.25	1.65 Å	2.32 Å	5.40 Å	0.10 Å
$p(\sqrt{3} \times \sqrt{3})$	0.33	1.72 Å	2.32 Å	4.68 Å	0.04 Å
DWcp	0.43	1.73 Å	2.29 Å	3.37 Å	0.13 Å
$c(2 \times 4)$	0.50	1.72 Å	2.26 Å	3.30 Å	0.12 Å
RuS_2	-	-	2.34 Å	2.23 Å	-

Further geometry information is reported in table 1. From the results shown in this table, we observe that the average S-Ru(0001) distance and the minimum S-Ru, atom-atom, distance does not change significantly from one surface reconstruction to the other. The S-S minimum distance, on the other hand, is consistently higher than the nominal values of 2.05Å, reported for the single S-S bond formation.[32] The short S-Ru bond length found in all the analyzed geometries suggests that the binding mechanism has a covalent nature (see also section3.2), whereas the dispersion forces only play a minor role in determining the final geometry arrangements. Indeed we have verified that geometry optimizations carried out with the dispersion forces switched-off lead to almost identical final structures. These facts suggest that the driving mechanism for the formation of the sulfur overlayer is dictated by the Ru surface, which imposes the hexagonal symmetry for low coverage values; the S atoms on the other hand tend to repel each other, as it happens in the formation of non commensurate monolayers on transition metals.[4] This last point justifies the fact that the hexagonal symmetry is lost as the quantity of S atoms is increased and that the adsorption sites are not all of the same kind for high coverage values.

Another interesting result is obtained by comparing the S-Ru distances obtained in our work with the nominal bond length found in Laurite (RuS_2),[33] which is a stable solid compound in which a covalent S-Ru bond is found. In the latter case, the bond length is 2.34Å, a value very similar to those found for the sulfur overlayers on Ruthenium, despite the fact that the coordination number changes from system to system. Notice, for example, that in RuS_2 each S_2 unit (with S-S bond length 2.2Å) is surrounded by 6 Ru atoms with a total of 4 bonds per S atom, whereas in the $p(2 \times 2)$ geometry, which exhibits very similar S-Ru bond length, the S atom is bonded to three Ru atoms only.

3.2 Charge transfer

In order to further clarify the S-Ru interaction mechanism, we have calculated the charge transfer upon adsorption of sulfur. To do so, we have applied the partitioning method of atoms in molecules, first introduced by Bader.[34,35] The results obtained are collected in Table2 and in Fig.3(a-d). First of all, we notice that, in all cases, the S atoms gain a

Table 2: Bader-based charge transfer. S_H and S_F refer to the S atoms located in *hcp* and *fcc* adsorption sites of the surface, respectively (see also Fig.2 and Fig.3)

		Gained e^- by S atoms			Lost e^- by topmost Ru	
Geometry	η	S atom	e^- gained	Average over S	Total	Average over Ru_{top}
$p(2 \times 2)$	0.25	S_H	0.45	0.45	0.45	0.11
$p(\sqrt{3} \times \sqrt{3})$	0.33	S_H	0.39	0.39	0.39	0.13
DWcp	0.43	S_H	0.36	0.35	1.04	0.15
		S_H	0.36			
		S_F	0.32			
$c(2 \times 4)$	0.50	S_H	0.33	0.32	1.28	0.16
		S_H	0.33			
		S_F	0.31			
		S_F	0.31			
RuS_2	-	Average over S 0.23			Average over Ru 0.45	

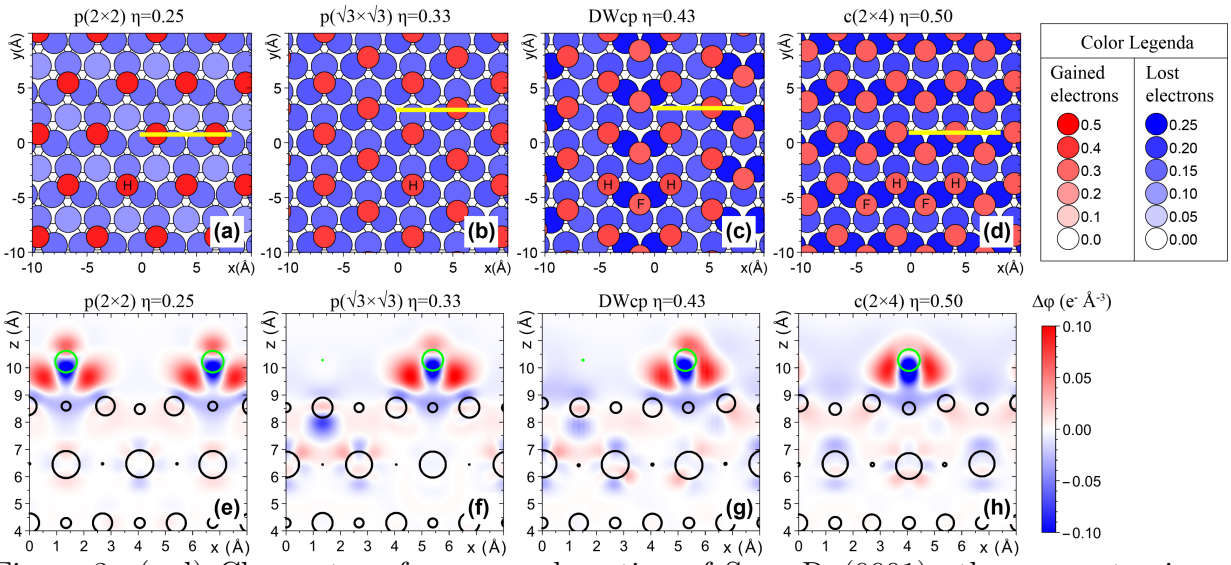

Figure 3: (a-d) Charge transfer upon adsorption of S on Ru(0001): the same atomic arrangements as in Fig.2 are displayed, the color of the spheres reflects the fraction of electron gained (red shades) or lost (blue shades) as indicated in the legenda; the *hcp* or *fcc* adsorption sites for the S atoms are marked by a "H" and a "F", respectively; the yellow line in each panel mark the exact location of the vertical cuts of $\Delta\phi$ shown in (e-h). (e-h) Vertical cuts of the $\Delta\phi$ given as density plots; the atom positions are marked by black (Ru) and green (S) circles, whose radius reflects the atom distance from the cut position.

fraction of electron, whereas the Ru atoms, actually only the Ru atoms of the topmost layer (Ru_{top}), tend to lose electrons, reflecting the fact that the S atom is more electronegative than the Ru atom. We observe that as the S density on the surface increases, the charge gained per S atom decreases. The most important results, however, are listed in the last two columns of Table2, where we report the total charge and the average charge per Ru atom that the topmost Ru layer transfers to the S atoms. We see a correlation between the charge transferred and the percentage of S atoms in the adlayer, with a maximum fraction of 1.28 electrons per unit cell transferred for the maximum surface coverage. The capability of the Ru(0001) surface to donate electrons was already proved in the past: monolayer graphene appears n-doped when adsorbed over the Ru(0001) surface.[36] Our results demonstrate that the adsorption of S atoms opens the possibility to alter this capability, as part of the charge of the topmost Ru atoms goes to the adsorbed S atoms. Moreover it suggests that the different S-Ru surfaces may exhibit a completely different chemical behavior when interacting

with molecules deposited on the surface or when adsorbing another adlayer, as for instance graphene.[9]

To complete the analysis of the charge transfer, we make use of Fig.3(a-d), in which we show that all the topmost Ru atoms participate in transferring electrons to S, even though not all of them contribute in the same way. In the case of the $p(\sqrt{3}\times\sqrt{3})$ geometry (Fig.3(b)), all the Ru atoms are equivalent, as all of them make a bond with the S atoms. In the $p(2\times2)$ geometry (Fig.3(a)), on the other hand, a slight difference is observed between the charge transfer by the four topmost atoms, with the Ru atoms forming the S-Ru bond contributing the most. More striking asymmetries are observed for the DWcp and the $c(2\times4)$ geometries. In the former, we see that the two Ru atoms that lay below the "v" arrangement of S atoms are the ones that transfer most of the charge, whereas in the latter, the Ru atoms that transfer the highest fraction of charge are organized in horizontal lines.

An interesting point of view is offered by the electron density redistribution ($\Delta\phi$), for which we show vertical cuts, given as density plots, in Fig.3(e-h). $\Delta\phi$ is defined as follows:

$$\Delta\phi(\mathbf{r}) = \phi_{S-Ru}(\mathbf{r}) - \phi_S(\mathbf{r}) - \phi_{Ru}(\mathbf{r}). \tag{1}$$

In (1) each ϕ is the total electron density as obtained in three (per each system) different DFT calculations: ϕ_{S-Ru} corresponds to the S-Ru system, whereas the other two electron densities are obtained from DFT calculations in which the Ru substrate (ϕ_S) or the sulfur overlayer (ϕ_{Ru}) had been removed, keeping unchanged the coordinates of the remaining atoms. Fig.3(e-h) show that a strong charge redistribution takes place in the vicinity of the S atoms. In particular, in Fig.3(e-h) we observe a region of charge depletion just below the S atoms, with regions of accumulation of electron density in the direction connecting the S atoms with the Ru atoms of the surface. In Fig.3(e-h) we have displayed $\Delta\phi$ cuts in the vicinity of *hcp* S atoms, however we have verified that cuts near *fcc* S atoms show a similar behavior. The observed charge displacement demonstrates that the S atoms are covalently

bonded to the surface.

3.3 Electronic Bands

The charge redistribution that takes place in the S-Ru interfaces directly affects their electronic properties, as shown in Fig.4, in which we depict the DFT band structure for the four long range ordered S-Ru phases analyzed in this work. To get more insight into the interface states, we have highlighted the one-electron states that exhibited a high localization of the wavefunction on the S layer or on the topmost Ru layer (Ru_{top}). To do so, we have proceeded as follows: for each one-electron state, labeled by band index n and quasi-momentum $\mathbf{k}$, characterized by band energy $\varepsilon_{n,\mathbf{k}}$ and wavefunction $\psi_{n,\mathbf{k}}$, we have calculated the probability density as function of the out of plane coordinate z, given by:

$$\rho_{n\mathbf{k}}(z) = \int_{2Duc} dxdy|\psi_{n\mathbf{k}}(x,y,z)|^2, \tag{2}$$

where the double integral was carried out over the in-plane unit cell (2Duc). Then for each state we calculated the integral

$$\int_{z_a}^{z_b} dz\rho_{n\mathbf{k}}(z), \tag{3}$$

choosing z_a and z_b so that the z position of either the S layer or the topmost Ru layer were included in the integration region. We hence have been able to assign to the interface region those one-electron states for which the weight given by (3) is at least 40%. Moreover we have further distinguished these states into pure S states (red dots in Fig.4), purely Ru_{top} (blue dots), or interface states, shown as dots with intermediate shades, determined by the relative weight of S and Ru_{top} contributions. At this point, we stress the fact that the DFT one-electron states only provide a qualitative view of the band structure of a system. To get quantitative accurate prediction of the energies and the wave functions more sophisticated Many Body methods must be used.

First of all, we notice that in all band plots one or more deep almost-flat bands are present

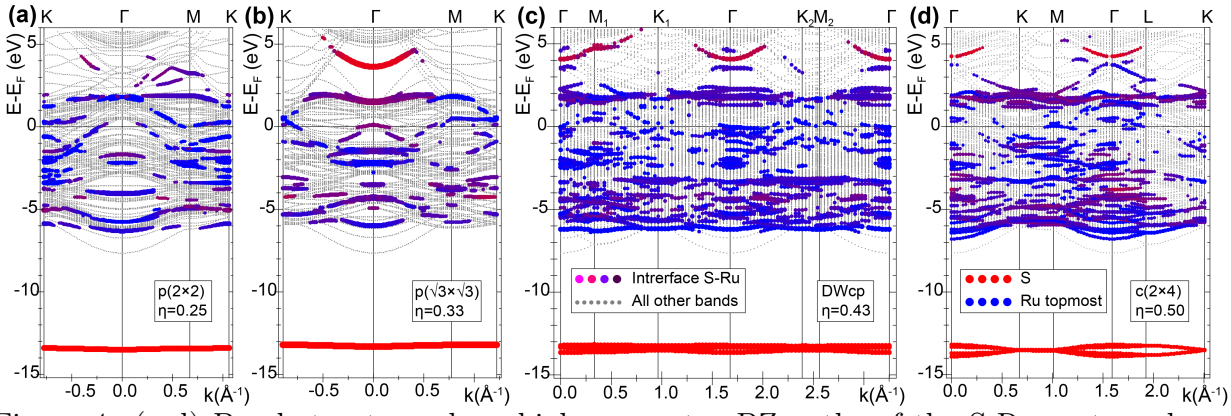

Figure 4: (a-d) Band structure along high symmetry BZ paths of the S-Ru system shown in Fig.2. The size of each point in the band plot marks how much a one electron state is localized in the interface region; a red point marks a purely sulfur state, a blue point marks a one electron state mostly localized on the topmost Ru layer, intermediate shades were used for mixed states, i.e. states whose ρ integral was high on both the S and the topmost Ru layer, whereas gray points were used for all the remaining one electron states.

for energies ~ -14eV. These bands are generated by the 3s sulfur atomic orbital and do not participate to the binding of the S atoms. Starting at ~ -6 eV and up to ~ 2 eV, we find a profusion of bands, mostly due to the d-bands of ruthenium. For $\eta \leq 0.33$ it is possible to follow the interface state along the BZ path. For higher coverage values it is more difficult to follow the dispersion of the interface states because of the larger number of atoms in the unit cell. On the other hand, in this energy window it is not possible to find a pure sulfur state, which means that the $3p$ sulfur atomic orbitals are all "engaged" in the formation of the chemical bond with the ruthenium surface.

The last remarkable feature in Fig. 4 is that for $\eta \geq 0.33$ a parabolic band, which has mainly a sulfur character, is present in the empty part of the band structure. In ref. 13 it was shown that it is possible to detect this one electron state by means of STS measurements, since this state causes the appearance of a peak in the spectrum that shifts with the sulfur coverage of the surface. Here we stress the fact that the energy of this parabolic state increases as the sulfur coverage increases, so that for $\eta = 0.33$ the vertex of the parabola is found at ~ 3.7eV; in the DWcp geometry it is found at 4.1 eV, and for $\eta = 0.50$ it is at 4.3 eV.

In order to get further insight into the electronic bands of the S-Ru interfaces, we have calculated the band structure (Fig. 5) of Sulfur monolayers[1], peeling the S atoms off the optimized S-Ru structure. Like in other one-atom thick flat bi-dimensional systems, due to the plane reflection symmetry, the relevant bands in the system are characterized by wave functions with even (σ bands) or odd (π bands) symmetry under reflection on the atomic plane. Hence, depending on the number of S atoms in the unit cell, the S monolayers present between one and four deep σ bands (not visible in Fig. 5) at energies $E - E_F \sim -10$eV. As already pointed out, these bands arise from the $3s$ electronic state of the isolated S atoms, and do not participate in the chemical bond between the S atoms and the Ru surface, since their energies are lower than the bottom of the Ru conduction band (found at -6eV with respect to the E_F). On the contrary, the $3p$ states of the S atom generate σ and π bands with energies close to E_F. These states are responsible for the chemical bond formation between the S atoms and the Ru surface, and produce interface states between S and Ru.

A deep knowledge of the system can be gained by observing the band dispersion in each of the different geometries. In the case of the $p(2\times2)$ structure, we find flat $E(k)$ dispersions for the σ and π bands, i.e., we see the band structure of periodically repeated quasi-isolated S atoms. On the other hand, the decrease of S-S distance leads to an increase of the S-S interaction, resulting in increasingly stronger band dispersion in the $p(\sqrt{3}\times\sqrt{3})$, DWcp and $c(2\times4)$ geometries, the most pronounced one being observed for the $c(2\times4)$ system.

In addition to the valence σ and π states, other interesting information can be obtained from the empty part of the band structures shown in Fig. 5. The most prominent feature is the presence of a quasi-continuum of bands starting at $\sim$ 5eV and having a parabolic dispersion with $\mathbf{k}$; these are the free electron solutions of the Kohn-Sham equations that form a continuum in the $L_z \to \infty$ limit, and can be used to estimate the energy of the vacuum level. Superimposed to the quasi-continuum it is possible to find other discrete one-electron states whose nature and properties depend on the specific symmetry of the

[1]It is worth mentioning that there is no evidence of the existence of freestanding planar 2D form of Sulfur.

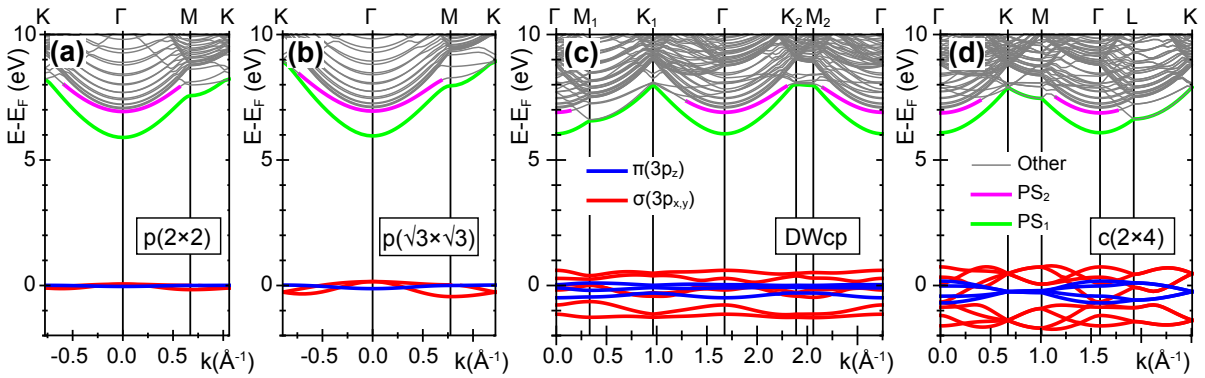

Figure 5: Band structure along high symmetry BZ paths (see Fig.2) for S *monolayers*: the S atom arrangements in each case is taken from the optimized position in the corresponding S-Ru system removing the Ru substrate. Red and blue thick lines are used for σ and π symmetry, respectively; green and magenta thick lines mark the PS_1 and PS_2 states, whereas all other bands appear as thin gray lines.

system.[37,38] In Fig. 5 two very remarkable bands (that we label PS_1 and PS_2) are found below the free electron threshold. In Fig. 6 we analyze the PS_1 and PS_2 one-electron states calculating their $\rho(z)$, by means of eq. (2) at the Γ point. We also add in each panel the $\rho(z)$ for the parabolic state observed in the corresponding S-Ru interfaces.

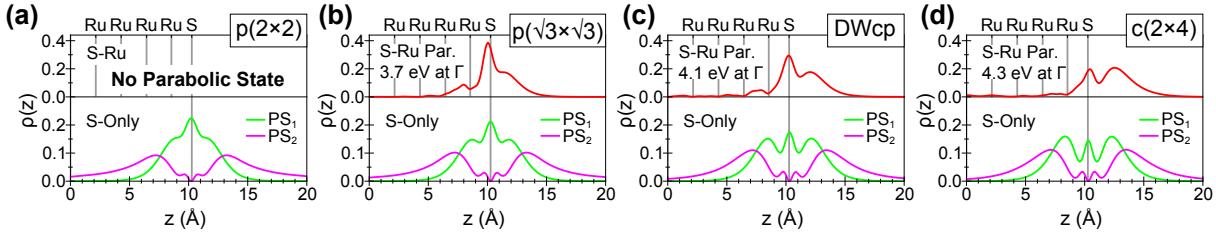

Figure 6: Comparison between the ρ calculated at the Γ point of the Parabolic state of the S-Ru interfaces and the PS_1 and PS_2 of the S monolayers. In each panel the parabolic S-Ru state is displayed in the top part (red line), whereas the PS_1 (green) and PS_2 (magenta) are shown in the bottom part; the vertical grid lines mark the position of the atomic layers.

Clearly PS_1 and PS_2 represent one-electron states characterized by a *bound motion* in the out-of-plane direction, since their wavefunction tends to zero for $z \to \pm\infty$. They are not obtained as a combination of atomic orbitals of the isolated S atoms, as demonstrated for freestanding graphene,[39] but a specific free electron model is needed to correctly account for them.[40] Indeed, as we have shown in Fig. 5, increasing the number of S atoms in the unit cell increases the number of σ and π bands, whereas only two PS bands are observed

in each system. Moreover, PS_1 and PS_2 have opposite symmetry with respect to the S plane; the $\rho_{PS_1}(z)$ presents a local maximum for $z = 0$, whereas ρ_{PS_2} has a node there. This fact suggests that the PS states are the first two states of a series of bound states below the vacuum level, which appear due to the potential well formed by the S layer, just as it happens in the series of image potential states observed in graphene,[15–17] or super atom states in carbon nanotube[18] and fullerenes.[19] In our case, such an infinite series is interrupted due to the incorrect asimptotic behavior of the one-electron potential of our DFT approach, which is not able to reproduce the image potential tail at high distances from the surface, but nevertheless is helpful in giving some qualitative properties.

4 Discussion

The comparison between PS_1 and PS_2 and the parabolic state in the corresponding S-Ru interface, carried out in Fig. 6, shows that both PS states are strongly affected and modified when the S monolayer is created on top of the Ru surface. They interact with the image states of the Ru slab, which leads to the formation of hybrid parabolic bands (the parabolic state itself is one of those). PS_1 and PS_2 interact as well with the interface states. In particular, as shown in ref 13, the presence of a high number of interface states at the Γ point explains the absence of a parabolic band in the $p(2 \times 2)$ geometry. In the other three S-Ru interfaces, we find a single parabolic band, whose vertex at the Γ point shifts toward high energies as the surface coverage increases. Looking at the corresponding ρ, we see that the parabolic bands are similar to the PS_1 states in the vacuum region, whereas in the Ru region their intensity rapidly drops.

Comparing Fig. 4 with Fig. 5 we can identify two remarkable features of the parabolic bands in the S-Ru interface: i) PS_1, which is the main contributor to the parabolic state in the S-Ru interfaces, is present in all the S monolayer systems, whereas the parabolic band is absent in the $p(2\times2)$ S-Ru interface; ii) PS_1 and PS_2 appear roughly at the same energy in all

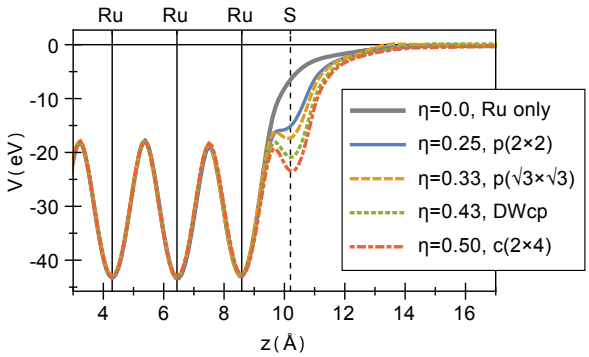

Figure 7: One dimensional averaged potentials for the S-Ru interfaces used in this work compared to the potential of a clean Ru surface; the vertical grid lines mark the position of the atomic layers.

the S monolayers, whereas, when present, the parabolic state exhibits a shift towards higher energies when the coverage increases. In ref 13 both facts were attributed to a competition between the band folding effect and the localization of the one-electron level on the S plane. Here we develop our analysis further, showing that it is possible to understand both results by using a simplified one-dimensional model.

In Fig. 7, we have plotted the averaged one dimensional potential[2] as a function of the out-of-plane coordinate for the four analyzed surfaces. From this figure we see that the presence of the S atoms induces changes in the potential due to the Ru surface. Nevertheless only for $\eta \geq 0.33$ a new minimum appears in the potential, related to the S layer, that facilitates the appearance of new localized states on the S layer.

This last point and the energy shift of the parabolic states are further clarified in Fig. 8, where we show some of the eigenvalues and eigenfunctions obtained after the diagonalization of the one-dimensional potential shown in Fig. 7. It is worth mentioning that the number of bound states, their energies, and the shape of their wavefunctions depends on the asymptotic conditions set for the potential. In our work we tried three different options that give qualitatively equivalent results: i) we set V=0 for $z < -6$Å and for $z > 15$Å (we will refer to the corresponding results with "Tail=0"); ii) we did not use any particular tail, taking

[2]These potentials are obtained averaging on the 2D unit cell the total potential felt by an electron (i.e. the Coulomb and the Exchange-Correlation potential).

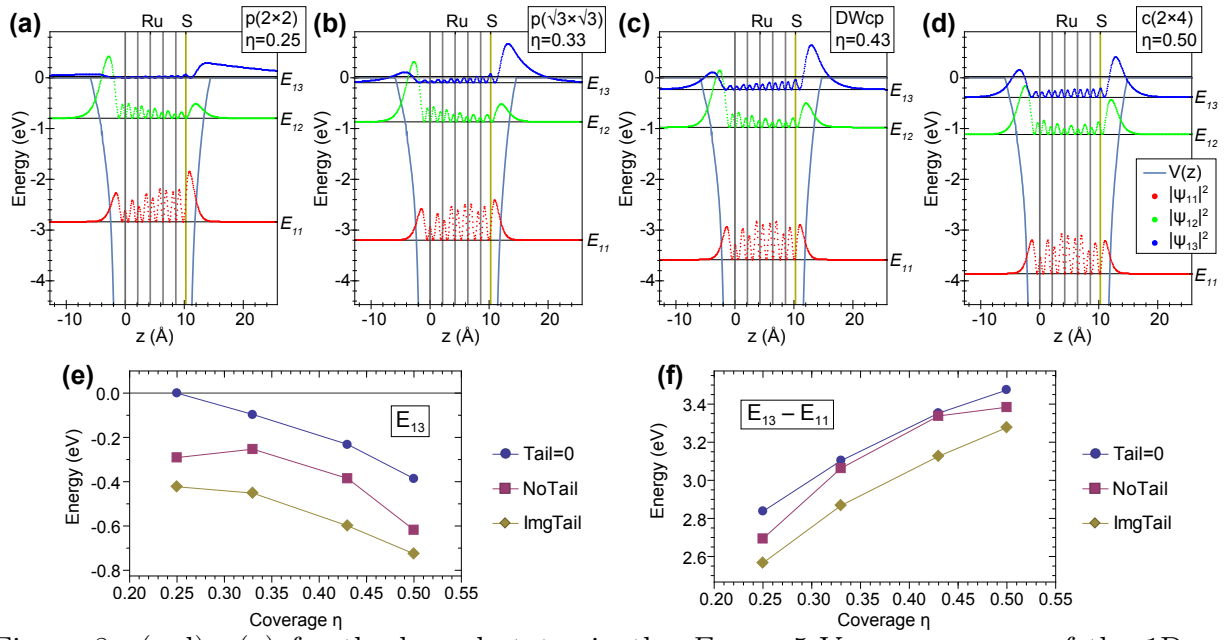

Figure 8: (a-d) $\rho(z)$ for the bound states in the $E > -5$eV energy range of the 1D average potential with the "Tail=0" option. The plot are placed vertically according to the corresponding eigenvalue; the vertical axis gives the value of these eigenvalues in eV and the energy scale for the averaged potential, which appears as a solid blue line; the vertical gridlines mark the position of the atomic layers. (e) Absolute value of the eigenvalue E_{13} for all the coverage values and all the "Tail" conventions. (f) Value of the eigenvalue E_{13} using as reference the E_{11} eigenvalue for all the coverage values and all the "Tail" conventions. In (e-f) the lines are a guide to the eye.

directly the averaged potential from the DFT calculations ("NoTail"); iii) we used a common image-potential like tail that drops like x^{-1} for $|x| \to \infty$ ("ImgTail")

In Fig. 8(a-d) we report the $\rho(z)$ for the 11^{th}, 12^{th}, and 13^{th} eigenfunctions that are the only states having energy higher than -5 eV when we use the "Tail=0" option. For all coverage values, ψ_{11} can be described as a slab state, as its $\rho(z)$ is distributed over the entire slab. On the contrary, ψ_{12} and ψ_{13} are surface-like states, since their $\rho(z)$ are peaked outside the slab; they are very close to the potential well states described in the previous section. These states resemble shape resonances found in atomic and molecular systems, and the method used here to uncover them, namely to impose different artificial forms of the potential in the asymptotic region, is common practice in atomic and molecular physics problems (see, e.g.,[41] and references therein). Interestingly in all four slabs the S layer causes that the two surface states are quite separated in energy, whereas a symmetric slab made only of Ruthenium has

two degenerate surface state. ψ_{12} is associated to the Ru termination of the slab whereas ψ_{13} is mostly peaked on the S side of the slab, hence it can be considered the one-dimensional counterpart of the parabolic state of Fig. 4. More interestingly, we see that, for the $\eta = 0.25$ coverage, the ψ_{13} state is very close to the vacuum level, which means that this state would be more "vulnerable" when the real three dimensional potential is considered; hence it is not surprising that for the $p(2 \times 2)$ S-Ru interface we do not find the parabolic state. We also observe that the absolute value of E_{13} decreases as η increases -see Fig. 8(e). This fact is consistent with the potential well formed by the S atoms, which becomes deeper as η increases. Interestingly we see that the parabolic state in the S-Ru interfaces follows the opposite behavior. As shown in Fig. 8(f), when these energies are referred to that of the last slab state (E_{11}), which can be considered as the equivalent of the Fermi level of the three dimensional system, all energies increase with coverage, in agreement with the behavior observed for the parabolic states. Therefore, the present analysis confirms that the origin of the parabolic states in S-Ru interfaces is the localization of the electron density around potential wells formed by the presence of the S atoms on the Ru surface. Finally, it is worth pointing out that the previous conclusion does not depend on the particular choice of the tail of the potential (see Fig. 8(e,f)).

5 Conclusions

In this manuscript, we have presented a DFT based study of the electronic properties of long range ordered S-Ru interfaces revealed by STM measurements. We have first described the structural properties of each S-Ru interface, focusing in particular on the nature of the interaction between the S atoms and the Ru surface. A comparative analysis of the S-Ru bond length and the charge transfer between the Ru surface and the S atoms have allowed us to determine that the Sulfur atoms make covalent bonds with the Ru surface in all the studied interfaces. More importantly, we have found that there is a direct relation between

the amount of charge transferred by the Ru surface and the sulfur density on the surface. This fact demonstrates that the sulfur adsorption can alter the capability of the Ru surface to further donate electrons to other adsorbed molecules or adlayers. It also suggests that each different surface could show a different chemical behavior, which can be fine tuned controlling the percentage of deposited sulfur. The covalent nature of the bond was also corroborated by the analysis of the DFT band structure of each system, in which we were able to identify the pure S one-electron states and the S-Ru interface states. Interestingly, in addition to a deep ($E - E_F \sim -14$eV) pure sulfur band, coming from the sulfur 3s orbital, our results show that it does not exist pure S states in the valence band, as all the sulfur 3p orbitals are engaged in forming covalent bonds with the ruthenium surface. More interestingly, in three of the four studied interfaces we have detected a parabolic state, mostly of S nature, whose energy increases when the percentage of sulfur atoms on the surface increases. From the study of the band structure of artificial monolayers of S atoms, obtained by removing the supporting Ru atoms, we were able to determine that this new parabolic state, recently revealed in scanning tunneling spectroscopy experiments, is in fact a potential well state, which appears on the surface when the amount of adsorbed sulfur is high enough to induce the presence of an additional potential well in the vicinity of the surface. Finally, we have presented a one-dimensional model that allowed us to account for the dispersing behavior of the parabolic state with the surface coverage.

Acknowledgement

We thank BSC-RES and CCC-UAM for allocation of computer time. Work partially supported by the MINECO Projects No. FIS2013-42002-R, FIS2016-77889-R and FIS2015-67367-C2-1-P, and the CAM Projects No. S2013/MIT-2850 and MAD2D S2013/MIT-3007. R. Bernardo-Gavito acknowledges a FPI grant BES-2011-050821; C. Díaz acknowledges the Ramón y Cajal program of the MINECO; D. Granados acknowledges RYC-2012-09864 and

ESP2015-65597-C4-3-R for financial support.

References

(1) Jürgens, D.; Held, G.; Pfnür, H. Adsorbate Induced Relaxations of S/Ru(0001): p(2 x 2) and p(sqrt3 x sqrt3)R30 Structures. *Surf. Sci.* **1994**, *303*, 77–88.

(2) Heuer, D.; Müller, T.; Pfnür, H.; Köhler, U. Determination of the Adsorption Site of Sulphur on Ru(0001) by STM. *Surf. Sci.* **1993**, *297*, L61–L67.

(3) Sokolowski, M.; Pfnür, H. Continuous Order-Disorder Phase Transitions of the p(2x2) and (sqrt3 x sqrt3)R30 Superstructures of Sulfur on Ru(001): Effective Critical Exponents and Finite Size Effects. *Phys. Rev. B* **1994**, *49*, 7716–7728.

(4) Jürgens, D.; Schwennicke, C.; Pfnür, H. Surface Structure Analysis of the Domain-Wall Phase of S/Ru(0001) Using an Efficient Parameter Optimization Method. *Surf. Sci.* **1997**, *381*, 174–189.

(5) Sokolowski, M.; Pfnür, H. Phase Transitions of the Striped Domain-Wall Phases of S on Ru(0001). *Phys. Rev. B* **1995**, *51*, 742–750.

(6) Schwennicke, C.; Jürgens, D.; Held, G.; Pfnür, H. The Structure of Dense Sulfur Layers on Ru(0001). I. The c(2x4) Structure. *Surf. Sci.* **1994**, *316*, 81–91.

(7) Sklarek, W.; Schwennicke, C.; Jürgens, D.; Pfnür, H. The Structure of Dense Sulfur Layers on Ru(0001). II. The (sqrt7 x sqrt7)R19.1 Structure,. *Surf. Sci.* **1995**, *330*, 11–19.

(8) Sutter, P.; Sadowski, J. T.; Sutter, E. A. Chemistry under Cover: Tuning Metal-Graphene Interaction by Reactive Intercalation. *Journal of the American Chemical Society* **2010**, *132*, 8175–8179.

(9) Bernardo-Gavito, R. *Intercalation of Sulfur in Epitaxial Graphene on Ruthenium(0001) Studied by means of Scanning Tunneling Microspocopy and Spectroscopy*; Universidad Autónoma de Madrid, 2016.

(10) Larciprete, R.; Lacovig, P.; Orlando, F.; Dalmiglio, M.; Omiciuolo, L.; Baraldi, A.; Lizzit, S. Chemical Gating of Epitaxial Graphene Through Ultrathin Oxide Layers. *Nanoscale* **2015**, *7*, 12650–12658.

(11) Alfonso, D. R. First-Principles Studies of H2S Adsorption and Dissociation on Metal Surfaces. *Surf. Sci.* **2008**, *602*, 2758–2768.

(12) Alfonso, D. R. Computational Studies of Experimentally Observed Structures of Sulfur on Metal Surfaces. *J. Phys. Chem. C* **2011**, *115*, 17077–17091.

(13) Pisarra, M.; Bernardo-Gavito, R.; Navarro, J. J.; Black, A.; Calleja, C. D. F.; Granados, D.; Miranda, R.; Martín, F.; de Parga, A. L. V. Coverage Evolution of the Unoccupied Density of States in Sulfur Superstructures on Ru(0001). *Appl. Surf. Sci.* **2018**, *433*, 300–305.

(14) Pisarra, M.; Pacilè, D.; Moras, P.; Sheverdyaeva, P. M.; Sindona, A.; Papagno, M.; Carbone, C. Electronic Structure of Epitaxial Graphene Grown on Stepped Pt(997). *Phys. Rev. B* **2014**, *89*, 195438.

(15) Armbrust, N.; Güdde, J.; Jakob, P.; Höfer, U. Time-Resolved Two-Photon Photoemission of Unoccupied Electronic States of Periodically Rippled Graphene on Ru(0001). *Phys. Rev. Lett.* **2012**, *108*, 056801.

(16) Silkin, V. M.; Zhao, J.; Guinea, F.; Chulkov, E. V.; Echenique, P. M.; Petek, H. Image Potential States in Graphene. *Phys. Rev. B* **2009**, *80*, 121408.

(17) Bose, S.; Silkin, V. M.; Ohmann, R.; Brihuega, I.; Vitali, L.; Michaelis, C. H.; Mallet, P.;

Veuillen, J. Y.; Schneider, M. A.; Chulkov, E. V. et al. Image Potential States as a Quantum Probe of Graphene Interfaces. *New Journal of Physics* **2010**, *12*, 023028.

(18) Hu, S.; Zhao, J.; Jin, Y.; Yang, J.; Petek, H.; Hou, J. G. Nearly Free Electron Superatom States of Carbon and Boron Nitride Nanotubes. *Nano Letters* **2010**, *10*, 4830–4838.

(19) Feng, M.; Zhao, J.; Huang, T.; Zhu, X.; Petek, H. The Electronic Properties of Superatom States of Hollow Molecules. *Accounts of Chemical Research* **2011**, *44*, 360–368.

(20) Posternak, M.; Baldereschi, A.; Freeman, A. J.; Wimmer, E. Prediction of Electronic Surface States in Layered Materials: Graphite. *Phys. Rev. Lett.* **1984**, *52*, 863–866.

(21) Borca, B.; Barja, S.; Garnica, M.; Sánchez-Portal, D.; Silkin, V. M.; Chulkov, E. V.; Hermanns, C. F.; Hinarejos, J. J.; Vázquez de Parga, A. L.; Arnau, A. et al. Potential Energy Landscape for Hot Electrons in Periodically Nanostructured Graphene. *Phys. Rev. Lett.* **2010**, *105*, 036804.

(22) Csányi, G.; Littlewood, P. B.; Nevidomskyy, A. H.; Pickard, C. J.; Simons, B. D. The Role of the Interlayer State in the Electronic Structure of Superconducting Graphite Intercalated Compounds. *Nat. Phys.* **2005**, *1*, 42–45.

(23) Sindona, A.; Plastina, F.; Cupolillo, A.; Giallombardo, C.; Falcone, G.; Papagno, L. Many Body Shake Up in X-ray Photoemission from Bundles of Lithium-Intercalated Single-Walled Carbon Nanotubes. *Surf. Sci.* **2007**, *601*, 2805–2809.

(24) Blöchl, P. E. Projector Augmented-Wave Method. *Phys. Rev. B* **1994**, *50*, 17953–17979.

(25) Kresse, G.; Joubert, D. From Ultrasoft Pseudopotentials to the Projector Augmented-Wave Method. *Phys. Rev. B* **1999**, *59*, 1758–1775.

(26) Perdew, J. P.; Burke, K.; Ernzerhof, M. Generalized Gradient Approximation Made Simple. *Phys. Rev. Lett.* **1996**, *77*, 3865–3868.

(27) Tkatchenko, A.; Scheffler, M. Accurate Molecular Van Der Waals Interactions from Ground-State Electron Density and Free-Atom Reference Data. *Phys. Rev. Lett.* **2009**, *102*, 073005.

(28) Monkhorst, H. J.; Pack, J. D. Special Points for Brillouin-Zone Integrations. *Phys. Rev. B* **1976**, *13*, 5188–5192.

(29) Vázquez de Parga, A. L.; Hernán, O. S.; Miranda, R.; Levy Yeyati, A.; Mingo, N.; Martín-Rodero, A.; Flores, F. Electron Resonances in Sharp Tips and Their Role in Tunneling Spectroscopy. *Phys. Rev. Lett. 80*, 357–360.

(30) Kelemen, S. R.; Fischer, T. E. Interaction of H2S with the Ru(001) Surface. *Surf. Sci.* **1979**, *87*, 53–68.

(31) Müller, T.; Heuer, D.; Pfnür, H.; Köhler, U. Domain Walls and Adsorbate-Step Interactions: an STM Study of Sulphur Layers on Ru(0001). *Surf. Sci.* **1996**, *347*, 80–96.

(32) Cottrell, T. L. *The Strengths of Chemical Bonds*, 2nd ed.; Butterworths: London, 1958; pp 15–17.

(33) Kratzig, A.; Zachäus, C.; Brunken, S.; Thomas, D.; Bogdanoff, P.; Ellmer, K.; Fiechter, S. RuS2 Thin Films as Oxygen-Evolving Electrocatalyst: Highly Oriented Growth on Single-Crystal FeS2 Substrate and their Properties compared to Polycrystalline Layers. *Phys. Status Solidi A* **2014**, *211*, 2020–2029.

(34) Bader, R. F. W. *Atoms in Molecules: a Quantum Theory*; Clarendon Press, 1994.

(35) Tang, W.; Sanville, E.; Henkelman, G. A Grid-Based Bader Analysis Algorithm without Lattice Bias. *J. Phys.: Condens. Matter* **2009**, *21*, 084204.

(36) Stradi, D.; Barja, S.; Díaz, C.; Garnica, M.; Borca, B.; Hinarejos, J. J.; Sánchez-Portal, D.; Alcamí, M.; Arnau, A.; Vázquez de Parga, A. L. et al. Electron localization

in epitaxial graphene on Ru(0001) determined by moiré corrugation. *Phys. Rev. B* **2012**, *85*, 121404.

(37) Pisarra, M.; Riccardi, P.; Sindona, A.; Cupolillo, A.; Ligato, N.; Giallombardo, C.; Caputi, L. Probing Graphene Interfaces With Secondary Electrons. *Carbon* **2014**, *77*, 796–802.

(38) Nazarov, V. U.; Krasovskii, E. E.; Silkin, V. M. Scattering Resonances in Two-Dimensional Crystals with Application to Graphene. *Phys. Rev. B* **2013**, *87*, 041405.

(39) Kogan, E.; Nazarov, V. U.; Silkin, V. M.; Kaveh, M. Energy Bands in Graphene: Comparison Between the Tight-Binding Model and *ab initio* Calculations. *Phys. Rev. B* **2014**, *89*, 165430.

(40) Kogan, E.; Silkin, V. M. Electronic Structure of Graphene: (Nearly) Free Electron Bands versus Tight-Binding Bands. *Phys. Status Solidi B* **2017**, *254*, 1700035.

(41) Macías, A.; Mendizábal, R.; Pelayo, F.; Riera, A.; Yáñez, M. Application of the Stabilization Method to the Molecular States of LiHe3+: Energies and Radial Couplings. *Phys. Rev. A* **1986**, *33*, 242–250.

TOC Graphic

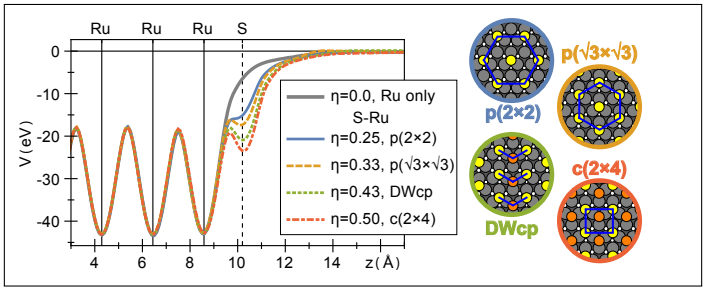
Ru
Ru
Ru
S
0
-10
-20
-30
-40
V (eV)
4
6
8
10
12
14
z (Å)
η=0.0, Ru only
S-Ru
η=0.25, p(2×2)
η=0.33, p(√3×√3)
η=0.43, DWcp
η=0.50, c(2×4)
p(2×2)
p(√3×√3)
DWcp
c(2×4)